Engineered Science
DOI: https://dx.doi.org/10.30919/es925

Exploring Point Defects in Rb_2O via First-Principles Calculations

Saleel Ahammad Saleel V. P.[1] and Eithiraj R. D.[2,*]

Abstract

Ab initio calculations for dirubidium oxide (Rb_2O) in antifluorite structure with four types of point defects, rubidium vacancy, oxygen vacancy, rubidium defect, and oxygen defect have been performed by the plane-wave self-consistent field based on density functional theory with generalized gradient approximation functional of Perdew-Burke-Ernzerhof exchange-correlation. For structural optimization, the Broyden-Fletcher-Goldfarb-Shanno algorithm is used. Defect formation energies are calculated under lattice relaxation for one unit cell of Rb_2O containing eight atoms of rubidium and four atoms of oxygen. For defect and vacancy structures, total energy, lattice constant, and vacancy formation energy are computed and discussed.

Keywords: Plane-wave method; Density functional theory; Total energy calculation; Vacancy formation energy.
Received: 30 May 2023; Revised: 14 July 2023; Accepted: 15 July 2023.
Article type: Research article.

1. Introduction

Defects in crystal are common. Their occurrence destroys the periodicity of the lattice structures in the crystals.[1,2] Among the various types of imperfections, consider her the situation where the lattice site reaming empty, known as vacancies. Oxygen (O) vacancies have a significant role on the physical and chemical properties of oxides and have been reported both experimentally and the theoretically.[3-7] Metal oxides have long been investigated with remarkable technology application as model-wide bandgap oxides. Extensive experimental studies of metal oxide defects and Face (F) center vacancy are carried out.[8-13] Point defects, such as atomic vacancies, play a crucial role in tailoring metal oxides properties.[14-16] By regulating the density and distribution of vacancies, a bandgap, conductivity, magnetism, *etc.*, can impact their physical properties. This can create exciting applications in the fields of energy storage and physical device applications.[17] Compounds with antifluorite crystal structure show rapid conductivity of particles and useful properties in energy storage, solid state batteries and gas detectors.[18-20] Various oxides of dilithium (Li_2O), disodium (Na_2O), dipotassium (K_2O), dirubidium (Rb_2O) crystallizing in an antifluorite structure.[18] In glass, optical, radiation shielding and ceramic applications, Rb_2O plays innovative utility role.[21] They have force in extensive thought due to their mechanical support, and moreover by their alternative outstanding and fascinating physical characteristics.[22-27] Using the spin-polarized density functional theory and the full potential linearized augmented plane wave plus local orbital method, the electronic structure and magnetic properties of Rb_2O alloys doped simultaneously with Cr and V transition elements are reported.[28] The vacancy formation energy calculations are carried out for Li_2O, Na_2O and K_2O using first principle study.[29-31] In this study, a series of detailed calculation for defect free, Rb defect, F center defect, Rb vacancy and O vacancy calculations for Rb_8O_4 using the *ab-initio* pseudopotentials approach density function theory (DFT) with the occupied valence orbitals represented by an expansion of the plane-wave method.

2. Computational methodology

The calculations were carried out by DFT, using the plane wave methods and the ultrasoft atomic pseudopotentials, as implemented in Quantum Espresso computational code.[32] The G vectors that allow for expansion are vectors of reciporcal lattice. At first, there is a need for an infinite number of vectors to describe the wave functions with infinite precision. However, the expansion of the planem waves can be truncated to a finite number of terms to limit the wave functions with a lower kinetic energy than an energy cut-off (E_{cutoff}).[33] The premise of the plane wave was increased to a 63 Ry energy cut-off. for wave functions and 513 Ry for charge density. The local-density approximation (LDA) makes use of the Perdew-Zunger (PZ)[34] and generalized gradient

[1] *Department of Physics, School of Advanced Sciences, Vellore Institute of Technology (VIT), Vellore 632 014, TN, India.*
[2] *Division of Physics, School of Advanced Sciences, Vellore Institute of Technology (VIT), Chennai 600 127, TN, India.*
[*] *Email:* eithiraj.rd@vit.ac.in (Eithiraj R. D.)

approximation (GGA) makes use of the Perdew-Burke-Ernzerhof (PBE)[35] for exchange and correlation effect. Used a k Monkhorst- Pack point mesh[36] of 4 × 4 × 4, in the first Brillouin zone. Using k-point sampling, we maintain an accuracy of 0.002 Ry. The Broyden-Fletcher-Goldfarb-Shanno (BFGS) method is used for structural optimizations.[37] The reference occupancy was chosen for rubidium $1s^2 2s^2 2p^6 3s^2 3p^6 3d^{10} 4s^2 4p^6 5s^1$ while the O premise orbitals are $1s^2 2s^2 2p^4$. Rb_2O defect free structure is show (Fig. 1), which crystallize in the antifluorite sutructure with a lattice constant 6.742 Å.[18] The DFT method has proven to be one of the most accurate methods for the computation of the electronic structure of solids.[38-44]

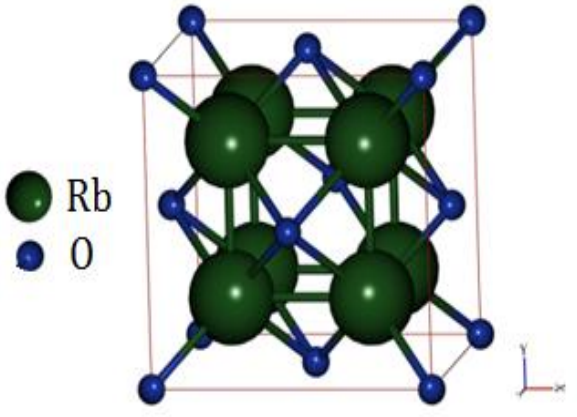

Fig. 1 Unit Cell of Rb_2O antifluotie structure.

3. Results and discussion

3.1 Total energy calculation

Different functional approximations are used, LDA and GGA, to calculate the relaxed and unrelaxed total energy for defect free structure, Rb defect, F centre defect, Rb vacancy and O vacancy. To create Rb defect, shifted one Rb atom from (0.25, 0.25, 0.25) to the BCC site. For the F-centre defect, the O atom from (0.0, 0.5, 0.5) site shifted to the BCC site. The vacancies of Rb and O were created by removal of atom from site site one by one. From Table 1, one observed that LDA consistently provides lower total energy values compared to GGA and also increases the total energy by increasing Rb and O vacancies in the 1 × 1 × 1 supercell structure of Rb_2O.

3.2 Relaxed lattice structure

Relaxed vacancy lattice structure shown in Figs. 2 & 3. Table 2 provides an overview of the lattice parameters for relaxed structures in the defect free crystal, Rb defects, F-center defects, and vacancies in the 1 × 1 × 1 supercell structure of Rb_2O. The calculated lattice constant for the defect-free structure in GGA is higher than in LDA. The initial atomic positions and lattice constant are set corresponding to the cubic lattice, while the lattice symmetries become tetragonal for Rb_2O_4 during the relaxed calculations. For $Rb_{(1)}$, $Rb_{(2)}$, $Rb_{(3)}$, $Rb_{(4)}$ vacancies, the displacement of the O atoms in the supercell structure is minimal; however, for $Rb_{(5)}$, $Rb_{(6)}$, $Rb_{(7)}$ vacancies, the O atoms migrate outward from the supercell structure. Because of the presence of Rb atoms in the tetrahedral site, the O atoms move outward. It also shows that the supercell structure is stable up to 50% Rb vacancy, becomes unstable after that point. For $Rb_{(6)}$ vacancy alone, cubic symmetry of the lattice transforms to tetragonal symmetry, and the c lattice is larger than the a and b lattices. In the case of the O vacancy, the displacement of the Rb atoms in the supercell structure is insignificant. For $O_{(1)}$ and $O_{(3)}$ vacancies, the lattice retains cubic symmetry, however for $O_{(2)}$ vacancies, the lattice shifts to tetragonal symmetry, with the c lattice being larger than the a and b lattices. This can be assigned to the c plane and atoms a and b axes to the asymmetry of the load densities. The Rb defect, F center defect

Table 1. Total energy calculation for defect free, Rb defect, Face centre defect, Rb vacancy, and O vacancy in Rb_2O 1 × 1 × 1 supercell structure.

System	Total Energy (Ry)			
	LDA		GGA	
	Unrelaxed	Relaxed	Unrelaxed	Relaxed
Rb_8O_4	-512.33233	-511.94267	-511.06638	-510.43728
Rb Defect	-512.11334	-511.94277	-510.81675	-510.43671
Face Centre Defect	-512.15236	-511.76464	-510.87690	-510.25583
Rb Vacancy				
$Rb_{(1)}$	-463.86131	-463.49404	-462.81308	-462.21482
$Rb_{(2)}$	-415.37756	-415.03692	-414.55002	-413.99826
$Rb_{(3)}$	-366.88042	-366.58253	-366.27183	-365.77450
$Rb_{(4)}$	-318.36871	-318.18341	-317.97703	-317.60699
$Rb_{(5)}$	-269.72071	-269.81542	-269.52179	-269.41332
$Rb_{(6)}$	-221.04944	-221.75933	-221.03847	-221.51392
$Rb_{(7)}$	-172.35010	-173.00724	-172.52193	-172.98513
O Vacancy				
$O_{(1)}$	-480.68801	-480.30763	-479.36886	-478.78071
$O_{(2)}$	-449.03295	-448.72388	-447.66839	-447.17302
$O_{(3)}$	-417.37678	-417.25041	-415.97060	-415.68452

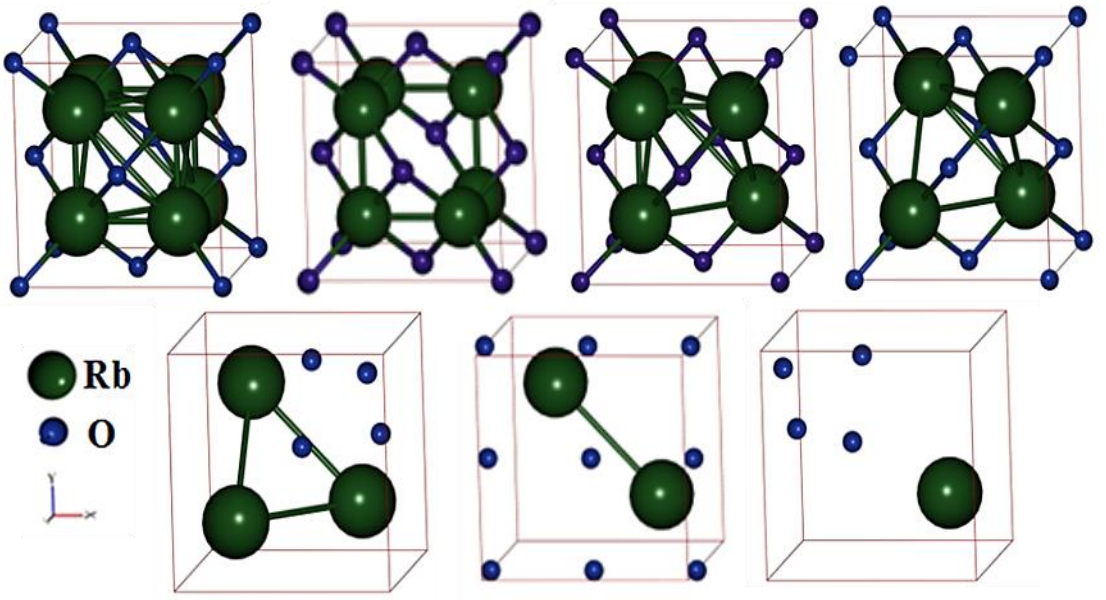

Fig. 2 Relaxed rubidium vacancy structure of Rb_8O_4.

Table 2. Lattice constant predicted by different functional for defect free, Rb defect, Face centre defect, Rb and O vacancy in Rb_2O 1 × 1 × 1 supercell structure.

System	Relaxed Lattice Constant (Å)					
	LDA			GGA		
	a	b	c	a	b	c
Exp. Lattice Constant 6.742 Å[18]						
Defect Free Rb_8O_4	5.813	5.813	5.813	5.858	5.858	5.858
Rb Defect	5.409	5.409	5.409	5.563	5.563	5.563
F Centre Defect	5.812	5.812	5.812	5.858	5.858	5.858
Rb Vacancy						
$Rb_{(1)}$	5.727	5.727	5.727	5.774	5.774	5.774
$Rb_{(2)}$	5.621	5.621	5.597	5.676	5.676	5.644
$Rb_{(3)}$	5.447	5.447	5.447	5.510	5.510	5.510
$Rb_{(4)}$	5.256	5.256	5.256	5.325	5.325	5.325
$Rb_{(5)}$	4.728	4.728	4.728	4.827	4.827	4.827
$Rb_{(6)}$	4.077	4.077	4.416	4.207	4.207	4.489
$Rb_{(7)}$	3.983	3.983	3.983	4.117	4.117	4.117
O Vacancy						
$O_{(1)}$	5.866	5.866	5.866	5.902	5.902	5.902
$O_{(2)}$	5.974	5.974	6.008	5.979	5.979	6.013
$O_{(3)}$	6.346	6.346	6.346	6.251	6.251	6.251

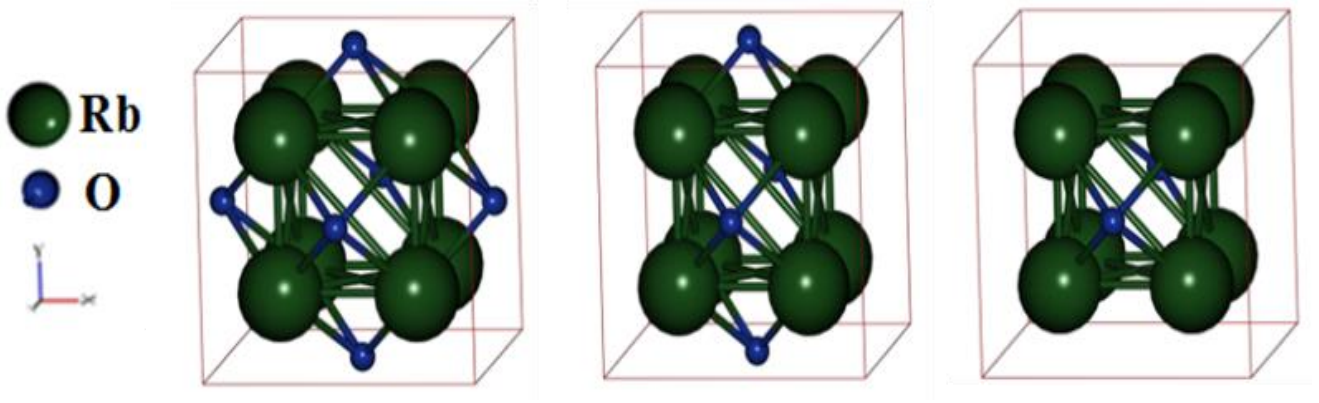

Fig. 3 Relaxed oxygen vacancy structure of Rb_8O_4.

and reaming concentration of Rb and O vacancies show cubic lattices in the relaxed structures. For O vacancies, a higher value of the lattice constant signifies the importance of O in the crystal system.

3.3 Vacancy relaxation volume

From Table 3, the Rb imperfection does not show any difference in volume in the relaxed structure compared to the defect free structure for LDA and GGA approximations. For the F-centre defect, the approximations of both LDA and GGA show positive volume variation compared to the defect-free structure, which expands strongly when O is moved to the BCC site. As the number of Rb vacancies increases, the volume decreases, and the number of O vacancies increases the volume increases, indicating that oxygens play a significant role.

3.4 Vacancy formation energy

The Rb vacancy formation energy E_c is calculated as;

$$E_c = E(Rb_7O_4) + E(Rb) - E(Rb_8O_4) \quad (1)$$

Where, E (Rb_7O_4) is the calculated total energy of the 1 × 1 × 1 supercell with Rb vacancies.

E (Rb) is the total energy of the free Rb atom.

E (Rb_8O_4) is the calculated total energy of the 1 × 1 × 1 supercell defect-free structure.

The O vacancy formation energy E_a is calculated as;

$$E_a = E(Rb_8O_3) + E(O) - E(Rb_8O_4) \quad (2)$$

Where, E (Rb_8O_3) is the calculated total energy of the 1 × 1 × 1 supercell with O vacancies. E (O) is the total energy of the free O atom. E (Rb_8O_4) is the calculated total energy of the 1 × 1 × 1 supercell defect-free structure. Table 4 provides a comparison of the vacancy formation energies between the LDA and GGA approximations. LDA consistently yields a higher value of RB vacancy formation energy than the GGA. The acquired values of the Rb vacancy formation energy using LDA and GGA were 258 and 156 kJ/mol, respectively. The $O_{(1)}$ vacancy formation energies calculated using LDA and GGA were 564 kJ/mol and 659 kJ/mol, respectively. It was observed that the energy required for the formation of O vacancies was much higher than that required for the formation energy of Rb vacancies. It is evident that vacancy formation energy increases with the increase in Rb and O vacancies resulting from the loss of atom stability in Rb_8O_4. The results show that mono-vacancies have the lowest energy of formation. The energy of vacancy formation increases as the number of vacancies increases.

3.5 Density of states

With the aid of GGA, the density of states of Rb_8O_4, Rb_7O_4 and Rb_8O_3 have been computed, and they are depicted in Fig. 4. Oxygen *p*-like state valence bands (VB) and potassium *s*-like state conduction bands (CB) formed a bandgap. Based on DOS calculations, O-2s states produce the lowest-lying bands in Rb_2O; above these bands, semi-core states like Rb-4*p* states appear. Rb *s*-like states make up the majority of the CB's bottom, which is separated from the rest by an energy gap. In ideal defect structure, the top valence band is dominated by *p*-like O states, whereas the lowest-lying band is dominated by *s*-like O states. The values of the calculated bandgap are compared to earlier theoretically derived findings in Table 5. The calculated bandgap value slightly deviates from experimental as well as theoretical results. For Rb vacancy in Rb_8O_4, the valence band maximum (VBM) is slightly shifted towards the E_F and maintain the same bandgap value like ideal structure. For O vacancy, the VBM and conduction band maximum (CBM) is getting closer to the E_F, have metallic behavior.

Table 3. Calculated equilibrium volume and volume variation of relaxed structure with different functional for defect free, Rb defect, Face centre defect, Rb and O vacancy in Rb_2O supercell structure.

System	LDA		GGA	
	Equilibrium Volume (Å^3)	Volume Variation (%)	Equilibrium Volume (Å^3)	Volume Variation (%)
Defect Free Rb_8O_4	196.427	0.000	201.024	0.000
Rb Defect	158.252	---	172.158	-1.706
F centre Defect	196.326	-0.516	201.024	0.000
Rb Vacancy $Rb_{(1)}$	187.837	-4.373	192.500	-4.240
$Rb_{(2)}$	176.841	-9.971	181.833	-9.547
$Rb_{(3)}$	161.611	-17.724	167.284	-16.784
$Rb_{(4)}$	145.200	-26.079	150.993	-24.888
$Rb_{(5)}$	105.690	-46.194	112.469	-44.052
$Rb_{(6)}$	73.402	-62.631	79.450	-60.477
$Rb_{(7)}$	63.187	-67.832	69.782	-65.287
O Vacancy $O_{(1)}$	201.849	2.760	205.587	2.270
$O_{(2)}$	214.418	9.150	214.955	6.930
$O_{(3)}$	255.564	30.107	244.258	21.507

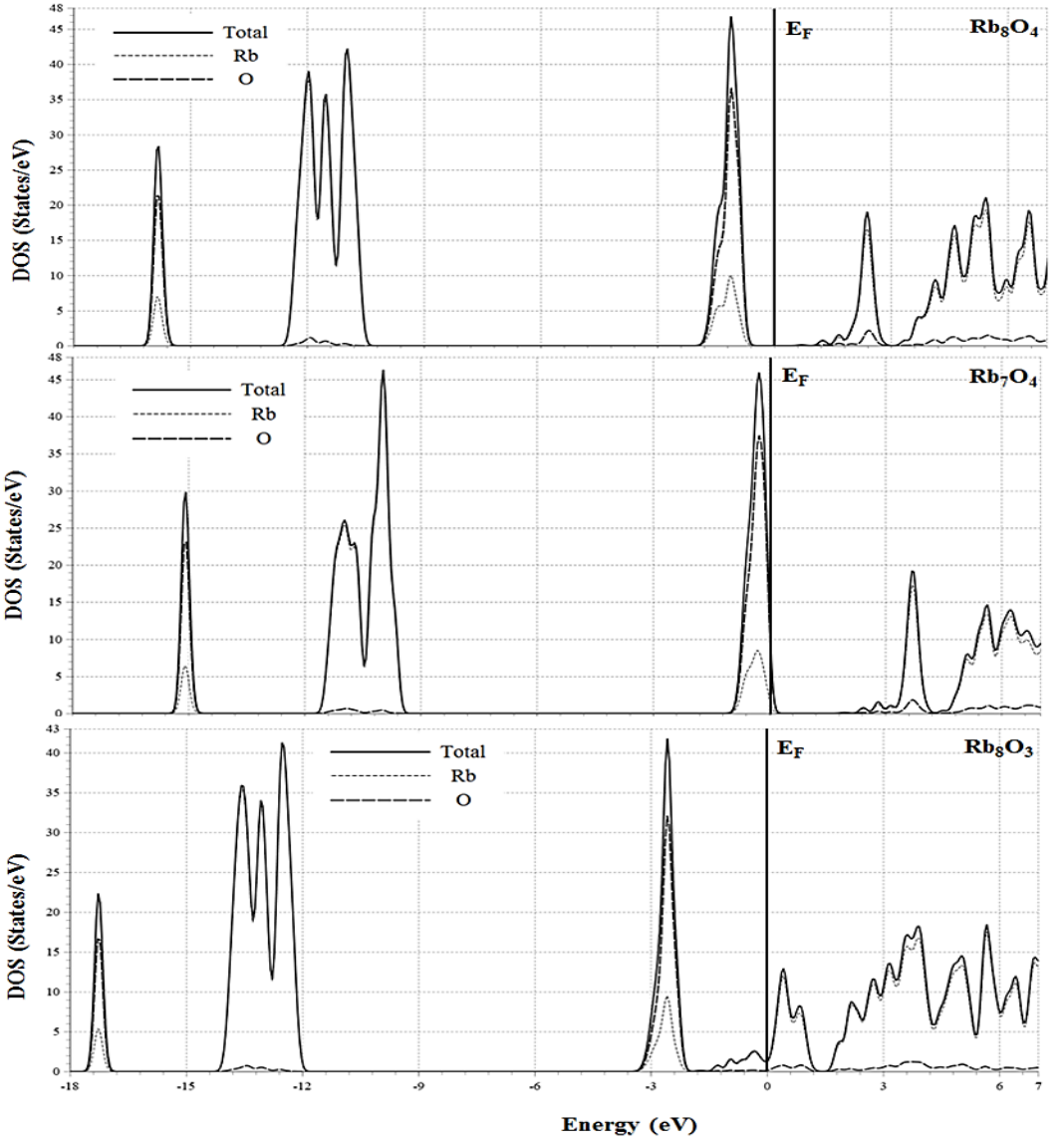

Fig. 4 Density of status of Rb_8O_4, Rb_7O4, Rb_8O_3 using GGA.

Table 4. Calculated vacancy formation energy (in kJ/mol) by different functional for Rb and O vacancy in Rb_2O supercell structure.

Rb_8O_4	Vacancy Formation Energy (kJ/mol)	
	LDA	GGA
Rb Vacancy		
$Rb_{(1)}$	258.39330	156.26435
$Rb_{(2)}$	527.92231	304.77790
$Rb_{(3)}$	793.87594	462.73917
$Rb_{(4)}$	987.26911	546.87318
$Rb_{(5)}$	1139.80432	665.34190
$Rb_{(6)}$	882.88202	397.42548
$Rb_{(7)}$	1539.64464	955.89520
O Vacancy		
$O_{(1)}$	564.18828	659.58968
$O_{(2)}$	1312.74969	1255.00144
$O_{(3)}$	1413.14312	1693.95019

Table. 5 Energy bandgap in Rb_8O_4.

	Present work (eV)		Other calculations (eV)	
Rb_8O_4	LDA	GGA	LDA	PBE/EV/WC with GGA
	1.52	1.56	1.55;[25] 1.49[27]	1.31;[26] 1.82;[27] 1.58[45]

4. Conclusion

With the occupied valence orbitals described by PWscf used density-function theory to calculate imperfection-free, Rb imperfection, O imperfection, Rb vacancy and O vacancy calculations for dirubidium oxide. The calculated lattice parameters for defect-free structure with the LDA and GGA for dirubidium oxide were lower (13%) than the experimental lattice parameter. The displacement of the O atoms in the supercell structure is insignificant for $Rb_{(1)}$, $Rb_{(2)}$, $Rb_{(3)}$, $Rb_{(4)}$ vacancies, however for $Rb_{(5)}$, $Rb_{(6)}$, $Rb_{(7)}$ vacancies, the O atoms migrate outward from the supercell structure. The presence of Rb atoms at the tetrahedral location causes the O atoms to migrate outward. It also demonstrates that the supercell structure is stable up to 50% Rb vacancy, but becomes unstable after exceeding 50% Rb vacancy. For $Rb_{(6)}$ vacancy alone, cubic symmetry (a = b = c) of the lattice transforms to tetragonal symmetry (a = b ≠ c), and the c lattice is larger than the a and b lattices. In the case of the O vacancy, the displacement of the Rb atoms in the supercell structure is insignificant. For $O_{(1)}$ and $O_{(3)}$ vacancies, the lattice retains cubic symmetry, however for $O_{(2)}$ vacancies, the lattice shifts to tetragonal symmetry (a = b ≠ c), with the c lattice being larger than the a and b lattices. The energy of O vacancy formation was higher than that of Rb vacancy formation. The ideal defect free structure has a bandgap of 1.52 eV for LDA and 1.56 eV for GGA, and shows semiconductor behaviour. It displays p-type semiconducting and metallic properties for Rb and O vacancies.

Conflict of Interest

There is no conflict of interest.

Supporting Information

Not applicable.

References

[1] J. M. Crawford, L. M. Slifkin, Point Defects in Solids, Plenum Press, New York, 1975.

[2] R. W. Siegel, Atomic Defects and Diffusion in Metals, North Holland Amsterdam, 1982.

[3] F. Trani, M. Causà, D. Ninno, G. Cantele, V. Barone, Density functional study of oxygen vacancies at the SnO_2 surface and subsurface sites, *Physical Review B*, 2008, **77**, 245410, doi: 10.1103/physrevb.77.245410.

[4] M. V. Ganduglia-Pirovano, A. Hofmann, J. Sauer, Oxygen vacancies in transition metal and rare earth oxides: current state of understanding and remaining challenges, *Surface Science Reports*, 2007, **62**, 219-270, doi: 10.1016/j.surfrep.2007.03.002.

[5] G. Pacchioni, L. Skuja, D. L. Griscom, Defects in SiO_2 and Related Dielectrics: Science and Technology, Springer publications, Springer Science & Business Media, 2012.

[6] A. Shluger, N. Itoh, Models of electronic defects and self-trapped excitons in Li_2O, *Journal of Physics: Condensed Matter*, 1990, **2**, 4119-4125, doi: 10.1088/0953-8984/2/18/008.

[7] I. A, Popov, Basic properties of the F-type centers in halides, oxides and perovskites, *Nuclear Instruments and Methods in Physics Research Section B: Beam Interactions with Materials and Atoms*, 2010, **268**, 3084-3089, doi: 10.1016/j.nimb.2010.05.053.

[8] E. Feldbach, R. Jaaniso, M. Kodu, V. P. Denks, A. Kasikov, P. Liblik, A. Maaroos, H. Mändar, M. Kirm, Luminescence characterization of ultrathin MgO films of high crystallinity prepared by pulsed laser deposition, *Journal of Materials Science: Materials in Electronics*, 2009, **20**, 321-325, doi: 10.1007/s10854-008-9599-z.

[9] R. C. Whited, W. C. Walker, Exciton spectra of CaO and MgO, *Physical Review Letters*, 1969, **22**, 1428-1430, doi: 10.1103/physrevlett.22.1428.

[10] L. A. Kappers, R. L. Kroes, E. B. Hensley, F^+ and F' centers in magnesium oxide, *Physical Review B*, 1970, **1**, 4151-4157, doi: 10.1103/physrevb.1.4151.

[11] G. H. Rosenblatt, M. W. Rowe, G. P. Williams, R. T. Williams, Y. Chen, Luminescence of F and F^+ centers in magnesium oxide, *Physical Review B*, 1989, **39**, 10309-10318, doi: 10.1103/physrevb.39.10309.

[12] A. Lushchik, T. Kärner, C. Lushchik, E. Vasil'chenko, S. Dolgov, V. Issahanyan, P. Liblik, Dependence of long-lived defect creation on excitation density in MgO single crystals, *Physica Status Solidi C*, 2007, **4**, 1084-1087, doi: 10.1002/pssc.200673785.

[13] Y. Chen, R. T. Williams, W. A. Sibley, Defect cluster centers in MgO, *Physical Review*, 1969, **182**, 960-964, doi: 10.1103/physrev.182.960.

[14] R. E. Mapasha, M. P. Molepo, R. C. Andrew, N. Chetty, Defect charge states in Si doped hexagonal boron-nitride monolayer, *Journal of Physics: Condensed Matter*, 2016, **28**, 055501, doi: 10.1088/0953-8984/28/5/055501.

[15] J.-Y. Noh, H. Kim, Y.-S. Kim, Stability and electronic structures of native defects in single-layer MoS_2, *Physical Review B*, 2014, **89**, 205417, doi: 10.1103/physrevb.89.205417.

[16] Saboura, Salehi, Atomic defect states in monolayers of MoS_2 and WS_2, *Surface Science*, 2016, **651**, 215-221, doi: 10.1016/j.susc.2016.05.003.

[17] G. Li, G. R. Blake, T. T. M. Palstra, Vacancies in functional materials for clean energy storage and harvesting: the perfect

imperfection, *Chemical Society Reviews*, 2017, **46**, 1693-1706, doi: 10.1039/c6cs00571c.

[18] E. Zintl, A. Harder, A. Dauth, Lattice Structure of the oxides, sulfides, selenides, and tellurides of lithium, sodium, and potassium, *Zeotscjrift fur Elektrochem*, 1934, **40**, 88, doi:10.1002/bbpc.19340400811.

[19] K. I. Cho, S. H. Lee, K. H. Cho, D. W. Shin, Y. K. Sun, Li_2O-B_2O_3-P_2O_5 solid electrolyte for thin film batteries, *Journal of Power Sources*, 2006, **163**, 223-228, doi: 10.1016/j.jpowsour.2006.02.011.

[20] M. Jamal, G. Venugopal, M. Shareefuddin, M. Narasimha Chary, Sodium ion conducting glasses with mixed glass formers NaI-Na_2O-V_2O_5-B_2O_3: application to solid state battery, *Materials Letters*, 1999, **39**, 28-32, doi: 10.1016/s0167-577x(98)00210-9.

[21] R. Kurtulus, C. Kurtulus, T. Kavas, Nuclear radiation shielding characteristics and physical, optical, mechanical, and thermal properties of lithium-borotellurite glass doped with Rb_2O, *Progress in Nuclear Energy*, 2021, **141**, 103961, doi: 10.1016/j.pnucene.2021.103961.

[22] K. Kunc, I. Loa, A. Grzechnik, K. Syassen, Li_2O at high pressures: structural properties, phase-transition, and phonons, *Physica Status Solidi (b)*, 2005, **242**, 1857-1863, doi: 10.1002/pssb.200461786.

[23] A. Lazicki, C.-S. Yoo, W. J. Evans, W. E. Pickett, Pressure-induced antifluorite-to-anticotunnite phase transition in lithium oxide, *Physical Review B*, 2006, **73**, 184120, doi: 10.1103/physrevb.73.184120.

[24] G. Kalpana, B. Palanivel, M. Rajagopalan, Electronic and structural properties of alkaline-earth oxides under high pressure, *Physical Review B*, 1995, **52**, 4-7, doi: 10.1103/physrevb.52.4.

[25] R. D. Eithiraj, G. Jaiganesh, G. Kalpana, Electronic structure and ground-state properties of alkali-metal oxides-Li_2O, Na_2O, K_2O and Rb_2O: A first-principles study, *Physica B: Condensed Matter*, 2007, **396**, 124-131, doi: 10.1016/j.physb.2007.03.024.

[26] K. Bidai, M. Ameri, A. Zaoui, I. Ameri, Y. Al-Douri, First principle study of mechanical stability and thermodynamic properties of anti-fluorite Li_2O and Rb_2O under pressure and temperature effect, *Chinese Journal of Physics*, 2016, **54**, 678-694, doi: 10.1016/j.cjph.2016.08.010.

[27] M. Moakafi, R. Khenata, A. Bouhemadou, H. Khachai, B. Amrani, D. Rached, M. Rérat, Electronic and optical properties under pressure effect of alkali metal oxides, *The European Physical Journal B*, 2008, **64**, 35-42, doi: 10.1140/epjb/e2008-00286-6.

[28] M. El Amine Monir, H. Baltach, A. Abdiche, Y. Al-Douri, R. Khenata, S. Bin Omran, X. Wang, D. P. Rai, A. Bouhemadou, W. K. Ahmed, C. H. Voon, Doping-induced half-metallic ferromagnetism in vanadium and chromium-doped alkali oxides K_2O and Rb_2O: ab initio method, *Journal of Superconductivity and Novel Magnetism*, 2017, **30**, 2197-2210, doi: 10.1007/s10948-017-4021-9.

[29] V. P. S. A. Saleel, D. Chitra, K. Veluraja, R. D. Eithiraj, Ab-initio calculation for cation vacancy formation energy in anti-fluorite structure, *AIP Conference Proceedings*, Mumbai, India. Author(s), 2018, **1942**, 090006, doi: 10.1063/1.5028921.

[30] W. J. Yin, S. H. Wei, M. M. Al-Jassim, J. Turner, Y. Yan, Doping properties of monoclinic $BiVO_4$ studied by first-principles density-functional theory, *Physical Review B*, 2011, **83**, 155102, doi: 10.1103/PhysRevB.83.155102.

[31] V. V. P. Saleel, R. D. Eithiraj, Vacancy formation energy in Disodium Oxide at 0K, *International Journal of Nanoelectronics and Materials*, 2020, **13**, 653-658.

[32] P. Giannozzi, S. Baroni, N. Bonini, M. Calandra, R. Car, C. Cavazzoni, D. Ceresoli, G. L. Chiarotti, M. Cococcioni, I. Dabo, A. Dal Corso, S. de Gironcoli, S. Fabris, G. Fratesi, R. Gebauer, U. Gerstmann, C. Gougoussis, A. Kokalj, M. Lazzeri, L. Martin-Samos, N. Marzari, F. Mauri, R. Mazzarello, S. Paolini, A. Pasquarello, L. Paulatto, C. Sbraccia, S. Scandolo, G. Sclauzero, A. P. Seitsonen, A. Smogunov, P. Umari, R. M. Wentzcovitch, QUANTUM ESPRESSO: a modular and open-source software project for quantum simulations of materials, *Journal of Physics: Condensed Matter*, 2009, **21**, 395502, doi: 10.1088/0953-8984/21/39/395502.

[33] J. Kohanoff, Electronic Structure Calculations for Solids and Molecules, Cambridge University Press, Cambridge, 2006, doi: 10.1017/cbo9780511755613.

[34] J. P. Perdew, A. Zunger, Self-interaction correction to density-functional approximations for many-electron systems, *Physical Review B*, 1981, **23**, 5048, doi:10.1103/PhysRevB.23.5048.

[35] J. P. Perdew, J. A. Chevary, S. H. Vosko, K. A. Jackson, M. R. Pederson, D. J. Singh, C. Fiolhais, Atoms, molecules, solids, and surfaces: applications of the generalized gradient approximation for exchange and correlation, *Physical Review B*, 1992, **46**, 6671-6687, doi: 10.1103/physrevb.46.6671.

[36] H. J. Monkhorst, J. D. Pack, Special points for Brillouin-zone integrations, *Physical Review B*, 1976, **13**, 5188-5192, doi: 10.1103/physrevb.13.5188.

[37] S. R. Billeter, A. J. Turner, W. Thiel, Linear scaling geometry optimisation and transition state search in hybrid delocalised internal coordinates, *Physical Chemistry Chemical Physics*, 2000, **2**, 2177-2186, doi: 10.1039/a909486e.

[38] A. Hassan, M. Ismail, A. H. Reshak, Z. Zada, A. A. Khan, M. Fazal Ur Rehman, M. Arif, K. Siraj, S. Zada, G. Murtaza, M. M. Ramli, Effect of heteroatoms on structural, electronic and spectroscopic properties of polyfuran, polythiophene and polypyrrole: a hybrid DFT approach, *Journal of Molecular*

Structure, 2023, **1274**, 134484, doi: 10.1016/j.molstruc.2022.134484.

[39] Hongjian, Yu, Coupling ferroelectric polarization and anisotropic charge migration for enhanced CO_2 photoreduction, *Applied Catalysis B: Environmental*, 2021, **284**, 119709, doi: 10.1016/j.apcatb.2020.119709.

[40] R. Ullah, A. H. Reshak, M. A. Ali, A. Khan, G. Murtaza, M. AL-Anazy, H. Althib, T. H. Flemban, Pressure-dependent elasto-mechanical stability and thermoelectric properties of MYbF3 (M = Rb, Cs) materials for renewable energy, *International Journal of Energy Research*, 2021, **45**, 8711-8723, doi: 10.1002/er.6408.

[41] S. Tabassam, A. H. Reshak, G. Murtaza, S. Muhammad, A. Laref, M. Yousaf, A. M. Al Bakri, J. Bila, Co_2YZ (Y= Cr, Nb, Ta, V and Z= Al, Ga) Heusler alloys under the effect of pressure and strain, *Journal of Molecular Graphics and Modelling*, 2021, **104**, 107841, doi: 10.1016/j.jmgm.2021.107841.

[42] R. Singla, S. Kumar, T. A. Hackett, A. H. Reshak, M. K. Kashyap, Genesis of magnetism in graphene/MoS_2 van der Waals heterostructures via interface engineering using Cr-adsorption, *Journal of Alloys and Compounds*, 2021, **859**, 157776, doi: 10.1016/j.jallcom.2020.157776.

[43] D. M. Hoat, S. Amirian, H. Alborznia, A. Laref, A. H. Reshak, M. Naseri, Strain effect on the electronic and optical properties of 2D Tetrahexcarbon: a DFT-based study, *Indian Journal of Physics*, 2021, **95**, 2365-2373, doi: 10.1007/s12648-020-01913-1.

[44] M. Husain, N. Rahman, A. H. Reshak, Zulfiqar, A. Habib, S. Ali, A. Laref, A. M. M. Al Bakri, J. Bila, Insight into the physical properties of the inter-metallic titanium-based binary compounds, *The European Physical Journal Plus*, 2021, **136**, 624, doi: 10.1140/epjp/s13360-021-01590-x.

